J. Fluid Mech. (1976), *vol.* 76, *part* 4, *pp.* 755–782
Printed in Great Britain

Axisymmetric homogeneous turbulence: a comparison of direct spectral simulations with the direct-interaction approximation

By U. SCHUMANN

Kernforschungszentrum Karlsruhe, Institut für Reaktorentwicklung, 75 Karlsruhe, Postfach 3640, West Germany

AND J. R. HERRING

National Center for Atmospheric Research, Boulder, Colorado 80303

(Received 23 October 1975)

The return to isotropy of homogeneous axisymmetric turbulence at $Re_\lambda \approx 28$ is studied by means of the direct spectral simulation (DSS) technique of Orszag & Patterson (1972) and the direct-interaction approximation (DIA) of Kraichnan (1959) as implemented by Herring (1974). The results of the two methods are compared for different initial degrees of anisotropy. The general agreement between the methods is good. Most of the discrepancies can be attributed to present technical limitations in implementing both schemes. The DSS has been found to be superior for strong anisotropies, because the numerical method used for solving the DIA equations is limited in its angular resolution. For small anisotropies the angular anisotropy becomes less important and the DIA results are accurate; in this case the DIA seems to be superior as it is free from the statistical uncertainties inherent in the DSS method. With respect to a return-to-isotropy study these statistical errors are large, in particular for small anisotropies. The physical interpretation of the angular energy distribution is discussed also. The numerical results and theoretical considerations for the DIA equations show that one should retain angular moments at least up to the fourth in order to obtain accurate values of the Rotta constant at moderate anisotropies.

1. Introduction

This paper investigates homogeneous axisymmetric turbulence. Results of direct spectral simulations (DSS) based on the numerical technique of Orszag & Patterson (1972) are compared with statistically equivalent results from the direct-interaction approximation (DIA) of Kraichnan (1959). The extension of the DSS to study the effect of pressure fluctuations will be described by Schumann & Patterson (1976*a*), who will also report certain results for anisotropic turbulence (1976*b*). The method of solving the DIA, together with preliminary results, has been described by Herring (1974). The comparison of numerical experiment and theory in the present study is made at a rather modest value of $Re_\lambda \approx 28$ (this

restriction is dictated by the scatter in the DSS results). Our comparison includes gross measures of anisotropy (such as Rotta's (1951) return-to-isotropy rate) as well as detailed spectral information on the components of the Reynolds-stress tensor and its angular distribution.

The present paper focuses on an assessment of the accuracy of the DIA as a complete turbulence theory, free from empirical parameters. We plan, in a subsequent paper, to examine the implications of such a theory for practical turbulence problems in more detail.

Overall, the agreement between the DSS experiment and DIA theory is excellent: not a surprising conclusion if we recall the good agreement reported for equivalent isotropic turbulence (Herring & Kraichnan 1972) and the fact that anisotropic effects should be significant mainly in the energy range, in which the DIA is expected to be most accurate. The agreement between the DSS and DIA appears to be best for the spherically averaged components of the scalars of the Reynolds-stress spectrum tensor, and somewhat poorer for their higher angular harmonics. This discrepancy does not appear appreciably to affect the Rotta return rate.

The Rotta constant (defined as the fractional rate of decrease of anisotropy using a time scale comprised of the longitudinal length scale and turbulence energy) ranges for the runs considered from 0·7 to 0·8. This range of values is somewhat smaller than that usually adopted in phenomenological theories (cf. Launder *et al.* 1973). It is also somewhat smaller than the preliminary DIA results of Herring (1974), but his calculations use a more severely truncated angular representation than the present one. With regard to the fact that the computed rates are smaller than those of the phenomenological theories, we suggest that this discrepancy results because models must allow for boundary effects as well as for non-axisymmetric components of the Reynolds stresses, while the present study includes neither of these. Interestingly, the present results are not discordant with the original estimates of Rotta (1951).

In § 2, we review briefly the notation and concepts for describing axisymmetric turbulence, from the perspective of numerical simulation. A more complete account of these ideas is presented in Schumann & Patterson (1976*b*). Section 3 states the DIA equations, describing briefly the special ingredients appropriate to axisymmetric turbulence, and the technique for numerically solving these equations. The principles of this procedure are presented in Herring (1974). The general basis of the DIA is also described by Leslie (1973), Orszag (1976) and, of course, Kraichnan (1959, 1964). The comparison between theory and simulation is given in § 4. The results include gross measures of anisotropy, such as the Rotta return rate, as well as detailed spectral comparisons of the angular distribution of the Reynolds stress. Section 5 presents a discussion of the physical meaning of the angular distribution. Section 6 discusses certain aspects of the DIA which are important in describing anisotropic turbulence but are not explicitly needed for isotropic turbulence. The important question here is the number of angular harmonics needed to represent accurately the Reynolds-stress spectrum (and associated Green's function) for a given degree of initial anisotropy.

2. Notation and concepts for the direct spectral simulation (DSS) of axisymmetric turbulence

We consider the decay of homogeneous turbulence in an incompressible fluid with constant viscosity ν. For computational convenience, periodic boundary conditions are imposed with periodic length L_{box} in each space direction. The smallest wavenumber is then $k_{\text{min}} = 2\pi/L_{\text{box}}$. The velocity vector $\mathbf{u}$ at the space position $\mathbf{x}$ at time t may be expanded in a Fourier series

$$\mathbf{u}(\mathbf{x},t) = \sum_{\text{all k}} \hat{\mathbf{u}}(\mathbf{k},t)\exp(i\mathbf{k}.\mathbf{x}), \tag{2.1}$$

where the $\hat{\mathbf{u}}(\mathbf{k}, t)$ are the (complex conjugate) spectral modes for the discrete set of wavenumber vectors $\mathbf{k} = k_{\text{min}}\,\mathbf{N}$; $\mathbf{N}$ is an integer vector. In the present numerical method we retain all wavenumbers $\mathbf{k}$ with $|\mathbf{k}| < k_{\text{max}}$, where

$$k_{\text{max}}/k_{\text{min}} = (242)^{\frac{1}{2}} \approx 15{\cdot}6.$$

This corresponds to 32^3 points being treated in real space. The spectral modes $\hat{\mathbf{u}}$ are determined by integrating the Navier–Stokes equations in time steps Δt. For technical details see Orszag & Patterson (1972). The pressure field is computed as described in Schumann & Patterson (1976*a*). The above value of k_{max} restricts accurate simulations to Reynolds numbers $Re_\lambda \lesssim 40$.

Initial values of $\mathbf{u}$ comprise a realization of an axisymmetric Gaussian ensemble whose axis of symmetry is $\mathbf{n} = (0, 0, 1)$.

The second-order ensemble-mean moments of $\hat{\mathbf{u}}$ in axisymmetric turbulence can be expressed by two scalar functions $\hat{\Phi}^\lambda(\mathbf{k}, t, t')$ (Herring 1974):

$$\langle \hat{u}_i(\mathbf{k},t)\,\hat{u}_j(-\mathbf{k},t')\rangle = \sum_{\lambda=1}^{2} \hat{\Phi}^\lambda(\mathbf{k},t,t')\,e_i^\lambda(\mathbf{k})\,e_j^\lambda(\mathbf{k}), \tag{2.2}$$

where the angular brackets denote the ensemble average and the unit vectors $\mathbf{e}^1$ and $\mathbf{e}^2$ are

$$\mathbf{e}^1(\mathbf{k}) = \mathbf{k}\times\mathbf{n}/|\mathbf{k}\times\mathbf{n}|, \quad \mathbf{e}^2(\mathbf{k}) = \mathbf{k}\times\mathbf{e}^1(\mathbf{k})/|\mathbf{k}\times\mathbf{e}^1(\mathbf{k})|. \tag{2.3}$$

The initial values $\hat{\mathbf{u}}(\mathbf{k}, 0)$ are determined in accordance with specified values of $\hat{\Phi}^\lambda(\mathbf{k}, 0, 0)$. They are chose such that the $\hat{\Phi}^\lambda(\mathbf{k}, 0, 0)$ are independent of the direction of $\mathbf{k}$, being given by

$$\hat{\Phi}^\lambda(\mathbf{k},0,0) = \frac{1}{2\pi k^2}\hat{E}(|\mathbf{k}|,0)\begin{cases}1-a, & \lambda=1,\\ a, & \lambda=2,\end{cases} \tag{2.4}$$

where a is an arbitrary parameter characterizing the initial anisotropy ($0 \leqslant a \leqslant 1$) and $\hat{E}(k, t)$ is the energy spectrum:

$$\hat{E}(k,t) \equiv \tfrac{1}{2}\hat{E}_{ii}(k,t). \tag{2.5}$$

The summation convention for repeated subscripts applies, and

$$\hat{E}_{ij}(k,t) = \int_0^\pi \int_{-\pi}^{\pi} \langle u_i(\mathbf{k},t)\,u_j(-\mathbf{k},t)\rangle\, k^2\,d\phi\,d\theta, \tag{2.6a}$$

with

$$\mathbf{k} \equiv k\{\sin\theta\cos\phi, \sin\theta\sin\phi, \cos\theta\}. \tag{2.6b}$$

Run	*SA*		*MA*	
Method	DSS	DIA	DSS	DIA
$\hat{E}(k,0)$ defined by	Equation (2.8)		Equation (2.8)	
k_{peak}/k_{max}, wavenumber of energy peak	0·3057	0·3333	0·3057	0·333
k_{max}/k_{min}, relative cut-off wavenumber	15·56	12·10	15·56	12·10
v_0, r.m.s. velocity at $t = 0$†	0·994	1·0	1·006	1·0
$Re_\lambda(t=0)$, Taylor-scale Reynolds number	28·07	28·07	28·47	28·47
$Re_L(t=0)$, integral-scale Reynolds number	35·98	34·99	36·56	35·72
$\Delta t v_0/\lambda(t=0)$, time step	0·04693	0·235	0·04738	0·237
$t_{max}v_0/\lambda(t=0)$ maximum time	3·7545		3·7908	
Number of realizations	3	—	8	—
$a = \Phi_0^2(t=0)/(\Phi_0^1(t=0)+\Phi_0^2(t=0))$, initial degree of anisotropy	0		0·25	

† In arbitrary units.

TABLE 1. Run specifications

The angle θ is defined with respect to the axis $\mathbf{n}$ such that

$$\mu = \cos\theta = \mathbf{k}.\mathbf{n}/|k|. \tag{2.7}$$

The DSS is run for two initial conditions labelled *SA* ('strong anisotropy'; this case is identical to case *A*2 discussed in Schumann & Patterson 1976*b*) and *MA* ('medium anisotropy'). In both runs, the initial energy spectrum is chosen to be

$$\hat{E}(k,0) = 16(2/\pi)^{\frac{1}{2}} v_0^2 k_{peak}^{-5} k^4 \exp[-2(k/k_{peak})^2], \tag{2.8}$$

where k_{peak} (the wavenumber for which $\hat{E}$ takes its maximum) and the initial root-mean-square (r.m.s.) velocity $v_0^2 = v^2(t=0) = \frac{1}{3}\langle \mathbf{u}.\mathbf{u}(\mathbf{x}, t=0)\rangle$ are given in table 1. The initial anisotropy is controlled by the parameter a [see (2.4)], which for run *SA* is

$$a = 0 \tag{2.9}$$

and for run *MA* is $a = 0{\cdot}25$.

The resultant initial anisotropy in terms of the $\hat{E}_{ij}$ is

$$\hat{E}_{33}/\hat{E}_{11} = 4a/(3-2a), \tag{2.10}$$

which takes the values

$$a = 0, 0{\cdot}4 \text{ for cases } SA, MA. \tag{2.11}$$

Also
$$\hat{E}_{22} = \hat{E}_{11}, \quad \hat{E}_{ij} = 0 \quad \text{if} \quad i \neq j. \tag{2.12}$$

From these initial conditions the flow decays slowly as it is damped by the viscous dissipation

$$\hat{\epsilon}_{ij}(k,t) = 2\nu k^2 \hat{E}_{ij}(k,t) \tag{2.13}$$

and approaches an isotropic state effected by the pressure–strain correlation $\hat{\Phi}_{ij}(k,t)$ and the inertial energy transfer $\hat{\Gamma}_{ij}(k,t)$. In terms of these quantities

$$\partial \hat{E}_{ij}(k,t)/\partial t = \hat{\Phi}_{ij}(k,t) + \hat{\Gamma}_{ij}(k,t) - \hat{\epsilon}_{ij}(k,t) \quad \text{for} \quad i,j = 1,2,3. \tag{2.14}$$

For the definitions of $\hat{\Phi}_{ij}$ and $\hat{\Gamma}_{ij}$ see Schumann & Patterson (1976*b*). Important characteristic properties are

$$\hat{\Phi}_{ii}(k,t) = 0 \tag{2.15}$$

and

$$\int_0^{k_{\max}} \hat{\Gamma}_{ij}(k,t)\,dk = 0 \quad \text{for} \quad i,j = 1,2,3. \tag{2.16}$$

If we integrate (2.6) over all wavenumbers k we get the real-space quantities

$$\begin{aligned} E_{ij}(t) &= \int_0^{k_{\max}} \hat{E}_{ij}(k,t)\,dk, \quad i,j = 1,2,3, \\ &\equiv \langle u_i(\mathbf{r},t)\,u_j(\mathbf{r},t)\rangle. \end{aligned} \tag{2.17a}$$

Similarly, the real-space wavenumber integrated values of the pressure–strain correlation, dissipation tensor, total energy and total energy dissipation are denoted, respectively, by

$$\Phi_{ij}(t), \quad \epsilon_{ij}(t), \quad E(t) = \tfrac{1}{2}E_{ii}(t), \quad \epsilon(t) = \tfrac{1}{2}\epsilon_{ii}(t). \tag{2.17b}$$

As discussed in detail in Schumann & Patterson (1976*a*, *b*), the rate of decay and return to isotropy are a function of the wavenumber k. As discussed by Herring (1974), the return to isotropy is also a function of the angle θ. Although the $\hat{\Phi}^{\lambda}(\mathbf{k}, t, t')$ are chosen to be independent of θ initially (for $t = t' = 0$), they become dependent on θ after a short time.

In order to examine this angular dependence and to check the DIA results in this respect, we express the angular dependence (as in Herring 1974) by means of angular moments $\hat{\Phi}^{\lambda}_l(\mathbf{k}, t, t')$ and Legendre polynomials $P_l(\mu)$:

$$\hat{\Phi}^{\lambda}(\mathbf{k},t,t') = \sum_{l=0}^{L} \hat{\Phi}^{\lambda}_l(|\mathbf{k}|,t,t')\,P_l(\mathbf{k}.\mathbf{n}/|\mathbf{k}|), \quad \lambda = 1,2, \tag{2.18}$$

$$P_0(\mu) = 1, \quad P_1(\mu) = \mu, \quad P_2(\mu) = \tfrac{3}{2}\mu^2 - \tfrac{1}{2}, \ldots. \tag{2.19}$$

As a consequence of axisymmetry and realizability all odd moments are zero. In the DIA runs described later, L is restricted to small values (usually $L = 2$). The angular moments with $l = 0$ and $l = 2$ are sufficient to describe the $\hat{E}_{ij}$ tensor (Herring 1974; Schumann & Patterson 1976*b*, appendix). The $\hat{\Phi}^{\lambda}_l$ computed by the DIA are compared with certain DSS moments $Z^{\lambda}_l(k)$, which are computed by the following least-squares fit:

$$\sum_{k_0 \leqslant |\mathbf{k}| < k_1} G(|\mathbf{k}|) \left[\hat{\Phi}^{\lambda}(\mathbf{k},t,t) - \sum_{l=0}^{L} Z^{\lambda}_l(t,k_0,k_1,G)\,P_l(\mu)\right]^2 (1-\mu^2)^{\frac{1}{2}} = \text{minimum}, \quad \lambda = 1,2, \tag{2.20}$$

where μ is as defined in (2.7) and the computations are for $L = 6$. The fitting procedure results in the usual formula

$$Z^{\lambda} = \frac{2l+1}{2} \int_{k_0}^{k_1} \int_{-1}^{1} G(k)\,P_l(\mu)\,\hat{\Phi}^{\lambda}(\mathbf{k}(\mu),t,t)\,d\mu \tag{2.21}$$

if the wavenumbers **k** are distributed continuously. The meaning of the resultant moments Z_l^λ depends upon the weighting function $G(k)$ and the wavenumber interval $[k_0, k_1]$. Small intervals $[k_0, k_1]$ are prohibited by statistical errors. We therefore compute moments $\Phi_l^\lambda(t) \equiv Z_l^\lambda(t, 0, k_{\max}, 1)$, which describe the angular distribution of the kinetic energy integrated over all wavenumbers k, and $\Omega_l^\lambda(t) \equiv Z_l^\lambda(t, 0, k_{\max}, 2\nu k^2)$, which describe the angular distribution of the energy dissipation rate integrated over all wavenumbers ($\lambda = 1, 2$; $l = 0, 2, 4, 6$).

Further parameters that characterize the flow statistics and are used for comparison are the integral length scale L_f, the Taylor microscale λ and the corresponding Reynolds numbers Re_L and Re_λ, as well as the skewness coefficient S and Rotta's (1951) return-to-isotropy coefficients C and C':

$$L_f(t) = \frac{\pi}{2v^2(t)} \int_{k_{\min}}^{k_{\max}} \frac{1}{k} \hat{E}(k, t)\, dk, \tag{2.22}$$

$$\lambda^2(t) = 15\nu\, v^2(t)/\varepsilon(t), \tag{2.23}$$

$$Re_L(t) = v(t)\, L_f(t)/\nu, \quad Re_\lambda(t) = v(t)\, \lambda(t)/\nu, \tag{2.24}$$

$$S(t) = \tfrac{1}{35}[15\nu/\varepsilon(t)]^{\frac{3}{2}} \int_0^{k_{\max}} \hat{\Gamma}_{iii}(k, t)\, k^2\, dk, \tag{2.25}$$

$$C(t) = -\Phi_{33}(t)\, E(t)/(\varepsilon(t) \Delta E(t)), \quad C'(t) = -\Phi_{33}(t)\, L_f(t)/(E^{\frac{1}{2}}(t)\, \Delta E(t)), \tag{2.26}$$

$$\Delta E(t) = \tfrac{2}{3} E_{33}(t) - \tfrac{1}{3}(E_{11}(t) + E_{22}(t)). \tag{2.27}$$

All these quantities show significant statistical fluctuations about their ensemble mean (also discussed by Riley & Patterson 1974). The average taken over the discrete values of the velocity field covered by the DSS is not large enough to make these mean values equal to the ensemble mean. This is true especially for those quantities that depend sensitively upon small values of the scalar wavenumber k, since the number of modes within a spherical shell in wavenumber space increases as k^2 (see Schumann & Patterson 1976*a*). Two means can be used to reduce the statistical uncertainties. First, we might shift the energy-containing region (at $k = k_{\text{peak}}$) to higher wavenumbers. Secondly, we can average over ensembles of realizations; each one is a run starting from initial values that are statistically equivalent but are constructed from different sets of random numbers. We apply both. The first method would result in large truncation errors (at $k = k_{\max}$), which are circumvented if the Reynolds number is reduced. The values of k_{peak} used here are twice those used for isotropic simulations by Orszag & Patterson (1972). For constant viscosity this would reduce the Reynolds number to about half its value. Since we want to study as high a Reynolds number as possible, we reduced the viscosity somewhat. As a consequence the truncation at the cut-off wavenumber is not completely negligible. However, we use the same value of $k_{\text{peak}}/k_{\min}$ and about the same value of $k_{\text{peak}}/k_{\max}$ in both the DIA and the DSS. Also, the return to isotropy is mainly controlled by the energy-containing region (see Schumann & Patterson 1976*b*; Herring 1974) and we may, therefore, allow some truncation errors at high wavenumbers since the energy range is of main interest. To reduce statistical scatter further, we obtain the DSS results from three realizations in case *SA* and

eight realizations in case MA. From these realizations it is possible to estimate the remaining statistical errors. If x_i, $i = 1, 2, \ldots, m$, are the results obtained from m realizations, the estimates for the mean value $\bar{x}$ and the standard deviation $\sigma(\bar{x})$ are

$$\bar{x} = \frac{1}{m}\sum_{i=1}^{m} x_i, \tag{2.28}$$

$$\sigma^2(\bar{x}) = \left(\sum_{i=1}^{m}(x_i - \bar{x})^2\right)\Big/ m. \tag{2.29}$$

(We shall give the results in the form $\bar{x} \pm \sigma(\bar{x})$ later.) Larger numbers m of realizations are necessary for weaker anisotropies if we are computing parameters that describe the departure from isotropy as, for example, $\Delta\Phi = \Phi_0^1 - \Phi_0^2$. If $\sigma(\Phi_0^\lambda)$, $\lambda = 1, 2$, are the standard deviations of Φ_0^λ, then the standard deviation of $\Delta\Phi$ is $\sigma^2(\Delta\Phi) = \sigma^2(\Phi_0^1) + \sigma^2(\Phi_0^2)$. In order to get significant results we require $\sigma^2(\Delta\Phi) < (\Delta\Phi)^2$. If one reduces $\Delta\Phi$ by a factor of $1/\alpha$, the number m of realizations must be enlarged by a factor of α^2 in order to get the same relative accuracy in $\Delta\Phi$. The initial value of $\Delta\Phi$ for case MA is half that for case SA; thus $\alpha = 2$. Therefore, the number of realizations should be four times larger for case MA in order to get the same accuracy as for SA. (This is even worse with respect to ΔE, defined in (2.27), which is changed by a factor of 2·333.) However, we restricted the number of realizations for practical reasons. (It should be noted that 13 min of computing time on NCAR's Control Data 7600 are required for one run of type SA or MA.) This also explains why the statistical accuracy decreases rapidly during the return to isotropy. We conclude that it is not practical to study weak anisotropies with the DSS.

3. The DIA for axisymmetric turbulence

The DIA for axisymmetric turbulence has been described elsewhere (Herring 1974), and we here summarize only certain important features of these equations. The approximation furnishes equations of motion for the two-time covariances $\hat{\Phi}^\lambda(\mathbf{k}, t, t')$ introduced in (2.2). The DIA equations for $\hat{\Phi}^\lambda(\mathbf{k}, t, t')$ are

$$\begin{aligned} &d\hat{\Phi}^\lambda(\mathbf{k}, t, t')/dt \\ &\quad = -\nu k^2 \hat{\Phi}^\lambda(\mathbf{k}, t, t') + \sum_{\mu,\nu}\int A_{\lambda\mu\nu}(\mathbf{k}, \mathbf{p}, \mathbf{q})\, d\mathbf{p} \int_0^{t'} ds\, g^\lambda(\mathbf{k}, t', s)\, \hat{\Phi}^\mu(\mathbf{p}, t, s)\, \hat{\Phi}^\nu(\mathbf{q}, t, s) \\ &\qquad + \sum_{\mu,\nu}\int B_{\lambda\mu\nu}(\mathbf{k}, \mathbf{p}, \mathbf{q})\, d\mathbf{p} \int_0^{t} ds\, g^\mu(\mathbf{p}, t, s)\, \hat{\Phi}^\lambda(\mathbf{k}, s, t')\, \hat{\Phi}^\nu(\mathbf{q}, t, s), \end{aligned} \tag{3.1}$$

where $\mathbf{q} = \mathbf{k} - \mathbf{p}$. The $g^\lambda(\mathbf{k}, t, t')$ are the Green's functions, satisfying

$$\begin{aligned} &dg^\lambda(\mathbf{k}, t, t')/dt + \nu k^2 g^\lambda(\mathbf{k}, t, t') \\ &\qquad = \sum_{\mu,\nu}\int d\mathbf{p} B_{\lambda\mu\nu}(\mathbf{k}, \mathbf{p}, \mathbf{q}) \int_0^{t} ds\, g^\mu(\mathbf{p}, t, s)\, g^\lambda(\mathbf{k}, s, t')\, \hat{\Phi}^\nu(\mathbf{q}, t, s), \end{aligned} \tag{3.2}$$

with the initial conditions

$$g^\lambda(\mathbf{k}, t', t') = 1.$$

In (3.1) and (3.2), $A_{\lambda\mu\nu}(\mathbf{k}, \mathbf{p}, \mathbf{q})$ and $B_{\lambda\mu\nu}(\mathbf{k}, \mathbf{p}, \mathbf{q})$ are coefficients whose form stems from the particular nonlinearity of the Navier–Stokes equations. They are given in Herring (1974, equations B6 and B7), and formulae for them are given in the appendix. Equations (3.1) and (3.2) reduce to the more familiar isotropic form of the DIA if we take $\hat{\Phi}^\lambda = \Phi(|\mathbf{k}|)$ and $g^\lambda = g(|\mathbf{k}|)$. Conditions on $A_{\lambda\mu\nu}(\mathbf{k}, \mathbf{p}, \mathbf{q})$ and $B_{\lambda\mu\nu}(\mathbf{k}, \mathbf{u}, \mathbf{q})$ which guarantee this are

$$\sum_{\lambda\mu\nu} A_{\lambda\mu\nu}(\mathbf{k}, \mathbf{p}, \mathbf{q}) = 8\pi kpqa(k, p, q)$$

and

$$\sum_{\lambda\mu\nu} B_{\lambda\mu\nu}(\mathbf{k}, \mathbf{p}, \mathbf{q}) = -8\pi kpqb(k, p, q),$$

with $a(k, p, q)$ and $b(k, p, q)$ given by

$$a(k, p, q) = \tfrac{1}{2}(b(k, p, q) + b(p, k, q))$$

and

$$b(k, p, q) = [(k^2 - q^2)(p^2 - q^2) + k^2p^2](pq/k)/d^2(k, p, q).$$

In these expressions, $d(k, p, q) \equiv k/\sin(p, q)$ is the diameter of the circle circumscribing the triangle whose sides are (k, p, q). We recall that in the present notation the total modal kinetic energy is $\hat{\Phi}^1(\mathbf{k}, t, t) + \hat{\Phi}^2(\mathbf{k}, t, t)$. Equations of motion for the time-diagonal values of $\hat{\Phi}^\lambda(\mathbf{k}, t, t)$ are derived by adding to (3.1) the equation obtained from (3.1) on interchanging t and t'.

Preliminary solutions of (3.1) and (3.2) have been presented by Herring (1974). There the angular representation of $\hat{\Phi}^\lambda(\mathbf{k})$ and $g^\lambda(\mathbf{k})$ was specified by a truncated Legendre series, as in (2.18). Except for certain studies with infinitely sharp wavenumber spectra, that study was limited to include only the $l = 0$, or spherically averaged, components of $\hat{\Phi}^\lambda$ and g^λ. The results obtained were in general accord with phenomenological estimates of anisotropic turbulence for an approximately self-similarly decaying spectrum; the rate of return, defined in terms of $C'(t)$ in (2.26), of an initially anisotropic field of homogeneous turbulence was about 1.3. The hypothetical linear nature of the decay of anisotropy was (approximately) confirmed by a numerical study of the A and B coefficients and the structure of (3.1) and (3.2) and by numerical integration of (3.1) and (3.2).

The present study focuses on the accuracy of the DIA as a technique for approximating initial-value solutions to the Navier–Stokes equations. For this purpose, we select an initial energy spectrum that is amenable to accurate numerical simulation even within the discrete and truncated wavenumber space used for the DSS, rather than one that has the virtue of preserving its shape during decay. Such a spectrum must have negligible energy near both the low and the high wavenumber cut-off; the spectrum given by (2.8) fits these requirements, provided the initial Reynolds number is not too large. At the same time, the rather formidable structure of (3.1) and (3.2) suggests that the number of angular harmonics treated must not be too large. Put differently, a calculation with a given angular harmonic cut-off L is accurate for an initial-value problem only if the initial departure from isotropy is less than an amount implied by L. The requirement of small anisotropy holds with respect both to the angular

harmonic representation and to the scalar difference $\hat{\Phi}^2 - \hat{\Phi}^1$. In the present paper, we truncate the angular expansion of (3.1) and (3.2) after $L = 2$. As we shall see, truncation at this level is adequate for moderately strong anisotropies, but is by no means adequate for all practical problems involving axisymmetric turbulence.

It is of interest to note the level of computer effort required to solve (3.1) and (3.2), as compared, for example, with the equivalent isotropic problem. The right-hand sides of (3.1) and (3.2) have the same time history and wavenumber convolution structure as the isotropic DIA, but the total number of independent terms is $8(L+1)^4$ times as large. Granted that numerical solutions of the DIA at moderate Reynolds numbers are now routine, the simplest anisotropic problem is thus still fairly sizeable, and requires additional economizing of the numerical procedures beyond those used, for example, in Herring & Kraichnan (1972) to fit into the same computer.

Our methods of numerically solving (3.1) and (3.2) are essentially the same as those of Herring & Kraichnan (1972) and Herring (1974). For the time stepping, we use Euler's modified method with an exact treatment of the viscous dissipation terms. Time integrals of the right-hand sides are done by Simpson's rule. The wavenumber integration is effected by assuming that the functions $\hat{\Phi}_l^\lambda(p)$, $g_l^\lambda(p)$, $\hat{\Phi}_l^\lambda(q)$ and $g_l^\lambda(q)$ can be interpolated in terms of cubic splines whose knots are k_n $(n = 1, 2, \ldots N)$, and then effecting the $dp\,dq$ integration by an appropriate Gaussian method. In the interpolation scheme, we take the arguments of the interpolated functions to be $x_0 \ln(k/k_0 + 1)$, with knots $k_n = k_0[\exp(x_0 n) - 1]$. Here x_0 is determined such that $k_N = k_{\max}$. This stretching concentrates the k_n's in the energy region, where spectral shapes change rapidly, and gives sparsely spaced points in the typically smoother dissipation range. For the present calculations, $N = 10$.

It should be noted that the numerical scheme outlined here is not strictly speaking energy conserving. However, the numerically treated p, q domain is one which properly corresponds to a systematic discard of interactions above a cut-off wavenumber $k_{\max}$. The interpolation procedure thus interpolates conservative transfer functions, although accurate numerical integration of the latter depends on having a sufficient density of knots k_n. Conversely, an insufficiency of knots is made manifest by non-zero estimates of the total energy transfer (2.16). We use the latter as a test of the numerical accuracy.

4. Comparison of DSS with DIA results

We compare numerical and theoretical results for the evolution of four types of statistics. First, we consider the integral quantities energy, dissipation and skewness. These are not *per se* measures of anisotropy, but their temporal evolution does depend on the initial anisotropy present. They have also been examined in earlier comparative studies of isotropic turbulence (e.g. in Orszag & Patterson 1972; Herring & Kraichnan 1972; Herring *et al.* 1973).

Second, we compare the results with respect to Rotta's return-to-isotropy rate $C'(t)$, defined by (2.26). The physical meaning of the above quantities and their

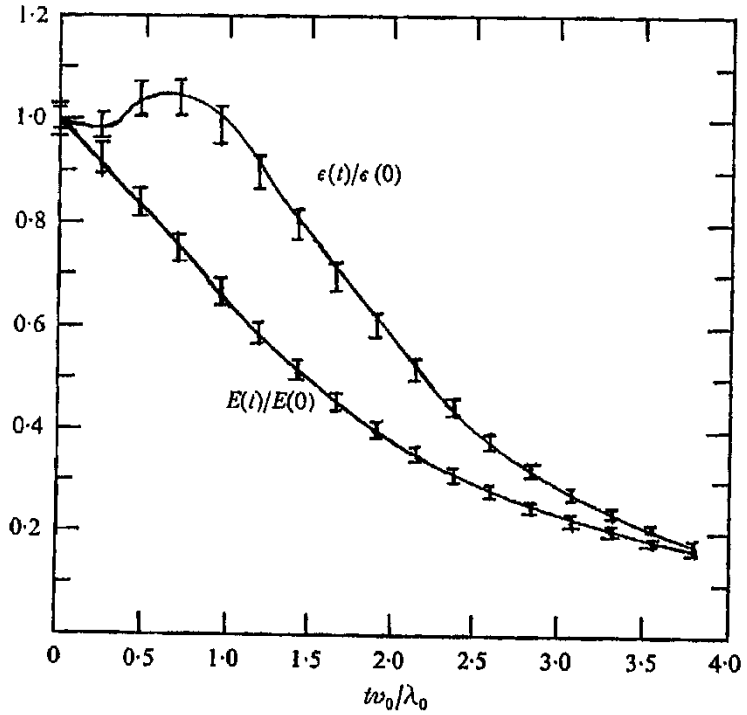

FIGURE 1. Energy $E(t)/E(0)$ and dissipation $\epsilon(t)/\epsilon(0)$ *vs.* time for case MA. The error bars indicate the DSS results, the curves are the DIA results.

time behaviour has been discussed elsewhere (Herring 1974; Schumann & Patterson 1976*a*, *b*).

Third, we examine the spectral measure of anisotropy $\hat{E}_{33}(k,t)/\hat{E}_{11}(k,t)$, defined by (2.6*a*). This quantity, as noted in § 2, depends only on the first two angular moments of the covariance spectrum tensor, but exhibits the wavenumber dependence of the return rate.

Finally, we compare results for the angular moments of energy (Φ^l_λ) and dissipation (Ω^l_λ) for $l = 0$ and 2. We also present DSS results for $l = 4$, in order to examine the convergence of the angular harmonic expansions. All DIA runs (except where otherwise stated) are for $L = 2$.

We compare the results obtained for strong [case SA, equation (2.11)], medium [case MA, equation (2.11)] and no [case $I2$] anisotropy. The last case has been investigated by Schumann & Patterson (1976*b*). Run $I2$ starts from the initial conditions (2.8), with $a = 0{\cdot}5$ [see (2.4)]. The DIA results for case $I2$ have been obtained with both the present code, designed for anisotropy, and the isotropic version used earlier (Herring & Kraichnan 1972). The differences between the results of these two codes for the same problem are insignificant or virtually zero.

Figure 1 shows the energy $E(t)/E(0)$ and dissipation $\epsilon(t)/\epsilon(0)$ *vs.* time t for case MA. The results for cases $I2$ and SA look similar except that the peak value of $\epsilon(t)/\epsilon(0)$ (at $tv_0/\lambda_0 \approx 0{\cdot}6$) decreases with growing anisotropy. The DSS runs give peak values of 0·98, 1·04 and 1·05 for initial values of $a = 0{\cdot}0$, 0·25 and 0·5. As indicated by the error bars, we see that the statistical errors in the DSS results

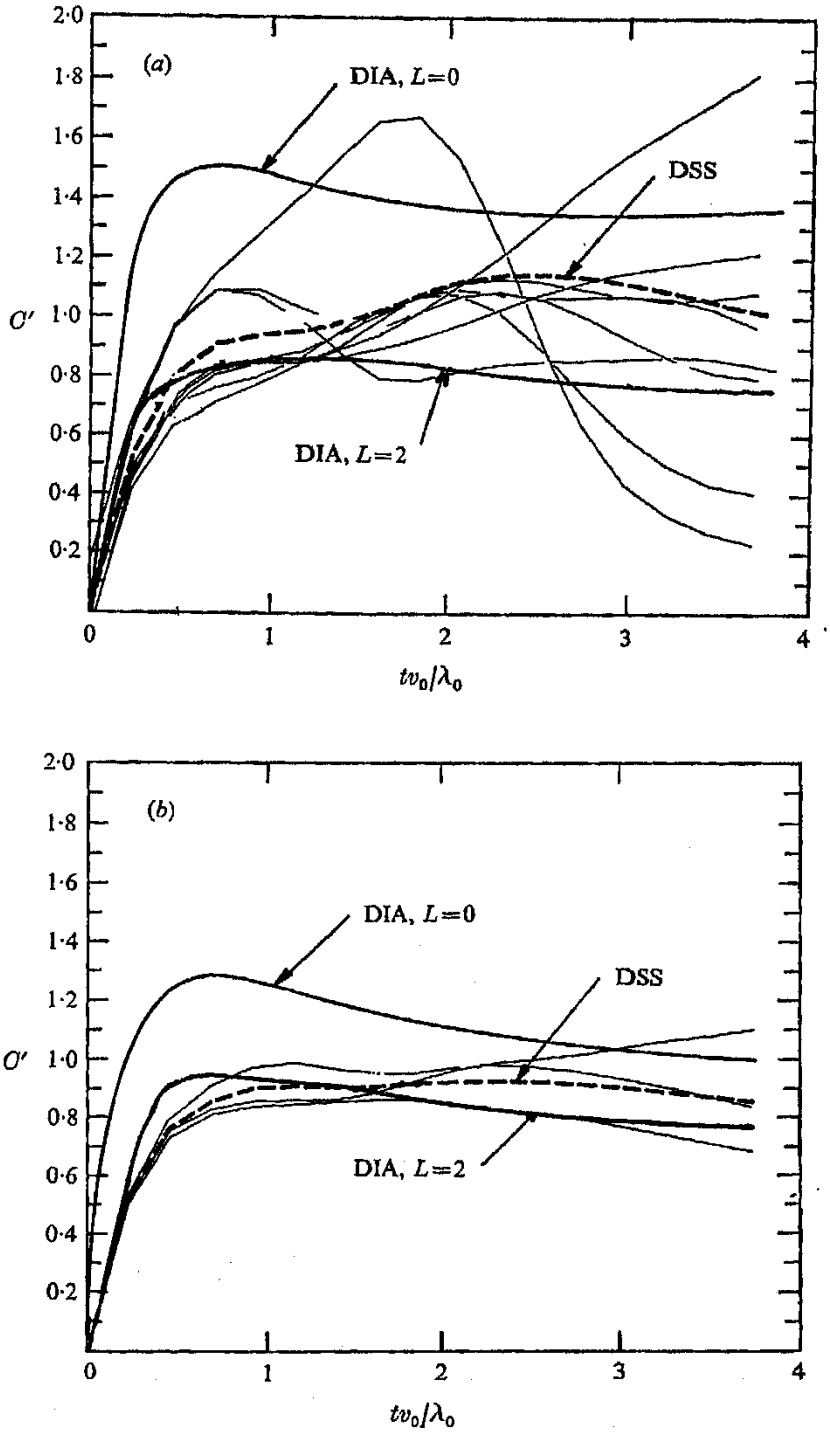

FIGURE 2. Rotta's return rate C' *vs.* time for (*a*) case MA and (*b*) case SA. The thin curves are the results obtained from the single DSS realizations.

for these integral quantities are less than 3 %. The DIA results are in good agreement with the DSS ones over the full time span of integration.

Rotta's return rate $C'(t)$ is shown in figures 2 (*a*) and (*b*). Here we present the DIA results for $L = 0$ and $L = 2$ together with the results obtained from all the single realizations of the DSS runs (thin curves) and the result found from the ensemble mean. First note the extremely large statistical fluctuations in the DSS results. A single realization could be completely misleading. The reason for the large statistical fluctuations in C' is not difficult to find. Note that C' is computed from four quantities [see (2.26)] each of which is contaminated with statistical errors. For example, at $tv_0/\lambda_0 = 0{\cdot}978$ for run MA (in arbitrary units)

$$\Phi_{33} = -0{\cdot}351 \pm 0{\cdot}053\,(15{\cdot}2\,\%), \quad \Delta E = 0{\cdot}214 \pm 0{\cdot}012\,(5{\cdot}4\,\%),$$
$$E = 1{\cdot}012 \pm 0{\cdot}036\,(3{\cdot}6\,\%), \quad L_f = 0{\cdot}272 \pm 0{\cdot}006\,(2{\cdot}2\,\%).$$

(The values in brackets give the percentage error.) The resultant value for C' is $0{\cdot}9 \pm 0{\cdot}15$ (17 %). We see that the largest errors arise from the pressure–strain correlation itself, which is basically determined by third-order correlations (Schumann & Patterson 1976*b*) whereas all other terms are defined in terms of second-order correlations. As shown by Orszag (1976) the statistical accuracy must be expected to decrease rapidly with growing order. At later times the errors in ΔE become more important.

The statistical errors seem to be small enough to allow the following conclusions from figures 2 (*a*) and (*b*). The agreement between the DSS and DIA is very good for both cases if we use the DIA with $L = 2$. Clearly, $L = 0$ results in a substantial overestimation of $C'(t)$. For case SA the agreement is not as good at small times, but improves somewhat at larger times, after the higher harmonics die away. The small-time overestimation of the return rate by the DIA is probably a result of our angular truncation procedure. As shown for simplified cases by Herring (1974), the inclusion of additional higher angular moments tends to decrease the resultant value of C'. Hence it appears that, for the DIA, $L = 2$ is too small for strong anisotropies; more evidence to support this conclusion will be given later.

The DSS results shown in figures 2 (*a*) and (*b*) also indicate a small decrease in C' with growing anisotropy; thus the DSS result for C' is about 5 % smaller for SA than for MA; this is, however, not entirely conclusive because of statistical uncertainties. For the DIA, a 20 % reduction is obtained on passing from MA to SA for the $L = 0$ truncation, while for $L = 2$, the DIA results indicate the opposite tendency: the values of C' are about 10 % larger for SA than for MA. This will be discussed further in § 5.2.

The wavenumber dependence of the return to isotropy, as measured by the ratio $r(k, t) \equiv \hat{E}_{33}(k, t)/\hat{E}_{11}(k, t)$ as a function of k at selected times, is given in figures 3 and 4. For $t = 0$ this ratio is as given by (2.10) and (2.11). [Equation (2.11) holds for the DSS runs for case MA within statistical errors only.] We see the return to the 'isotropic' value $r = 1$, with a larger return rate at high wavenumbers. At later times the inertial energy transfer, which is anisotropic owing to the anisotropy at low wavenumbers, retards the return to isotropy. Again, we see relatively large statistical errors for the DSS results; they are largest at small

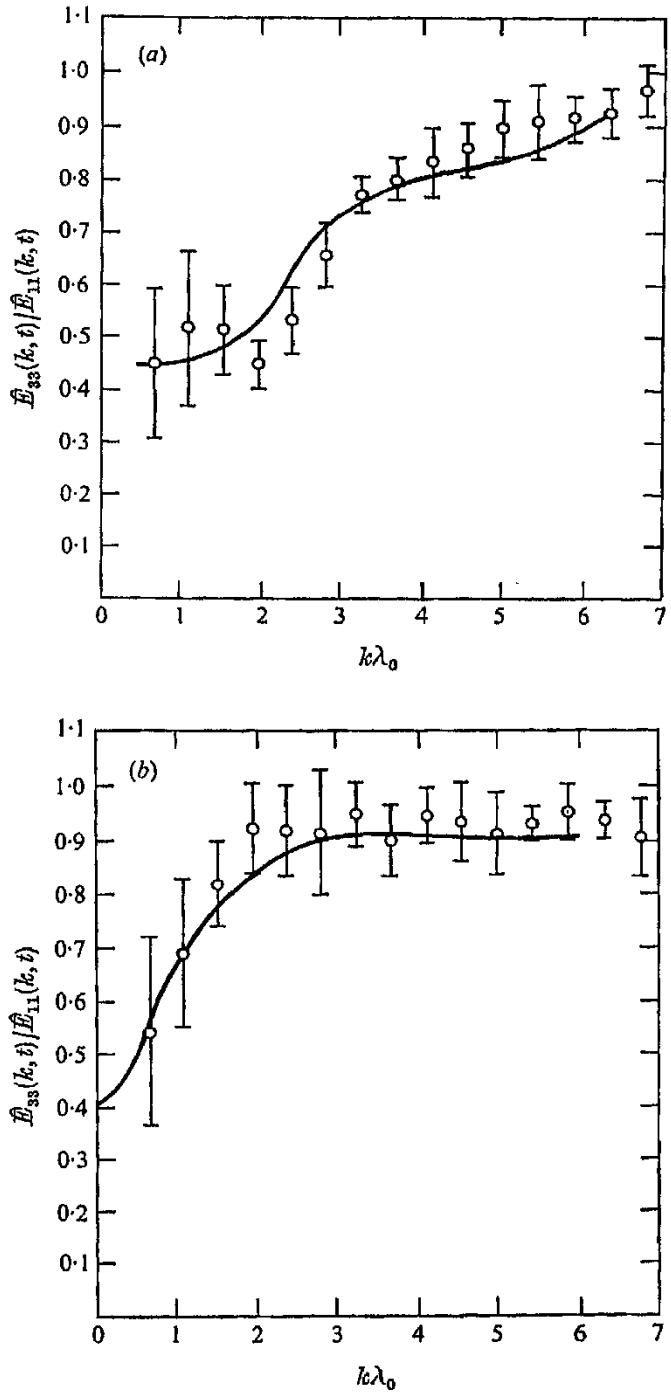

FIGURE 3. Energy ratio *vs.* wavenumber for case *MA* and times (*a*) $tv_0/\lambda_0 = 0{\cdot}948$ and (*b*) $tv_0/\lambda_0 = 3{\cdot}79$. Here, and in all subsequent figures, dots with error bars indicate DSS results; full curves represent DIA results.

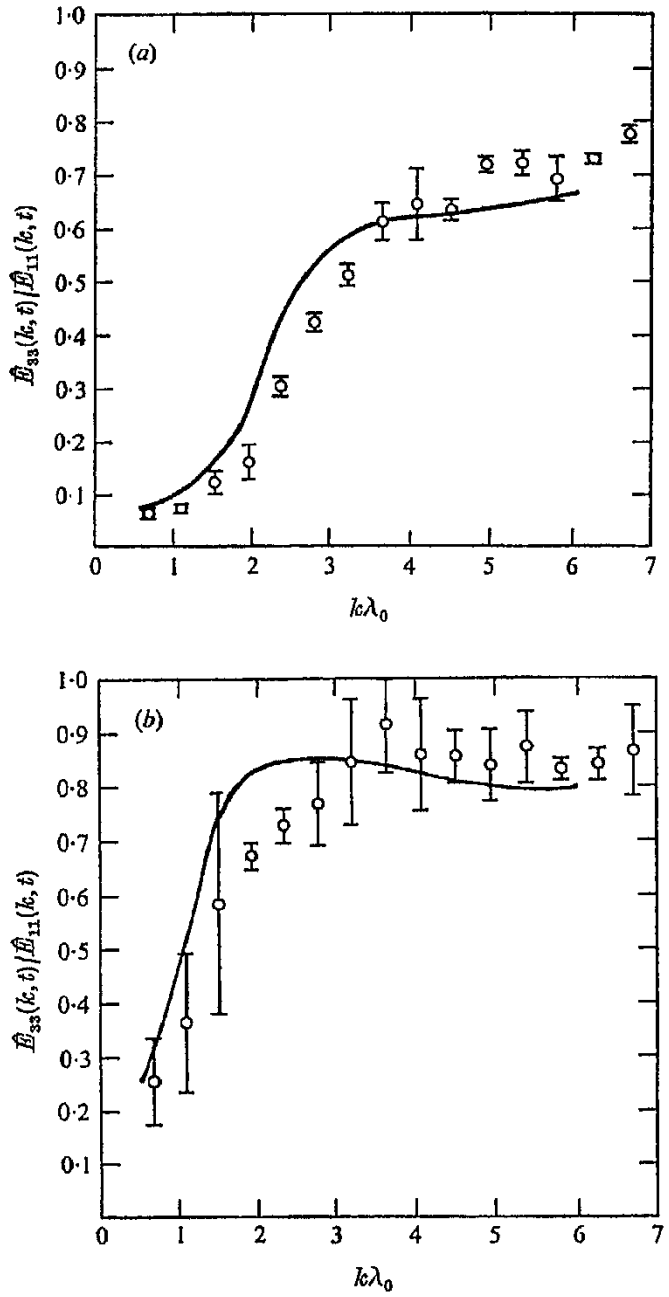

FIGURE 4. Energy ratio *vs.* wavenumber for case *SA* and times (*a*) $tv_0/\lambda_0 = 0{\cdot}939$ and (*b*) $tv_0/\lambda_0 = 3{\cdot}754$.

wavenumbers, where only a few modes are present. Nevertheless, the DIA and DSS results for case *MA* (figure 3) show good agreement at all times and wavenumbers. The DIA results are only slightly smaller than the DSS results, as expected from the smaller C' values noted above. Figures 4(*a*) and (*b*) (case *SA*) indicate that the DIA somewhat overestimates the return rate for moderate k and underestimates it for large k. Curiously, both theory and simulation show a larger departure from isotropy at very large k than for moderate k. This may

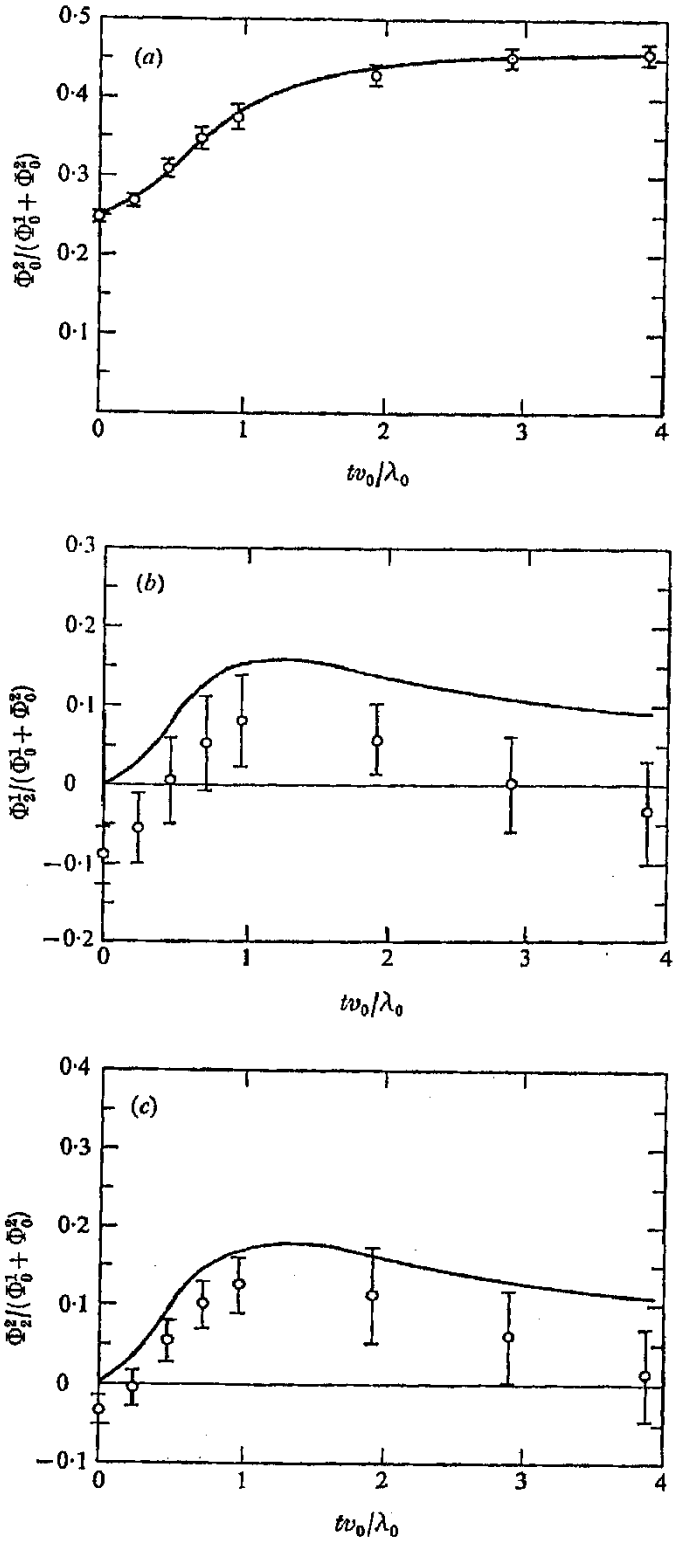

FIGURE 5. Energy moments *vs.* time for case MA. (*a*) $\Phi_0^2/(\Phi_0^1+\Phi_0^2)$. (*b*) $\Phi_2^1/(\Phi_0^1+\Phi_0^2)$. (*c*) $\Phi_2^2/(\Phi_0^1+\Phi_0^2)$.

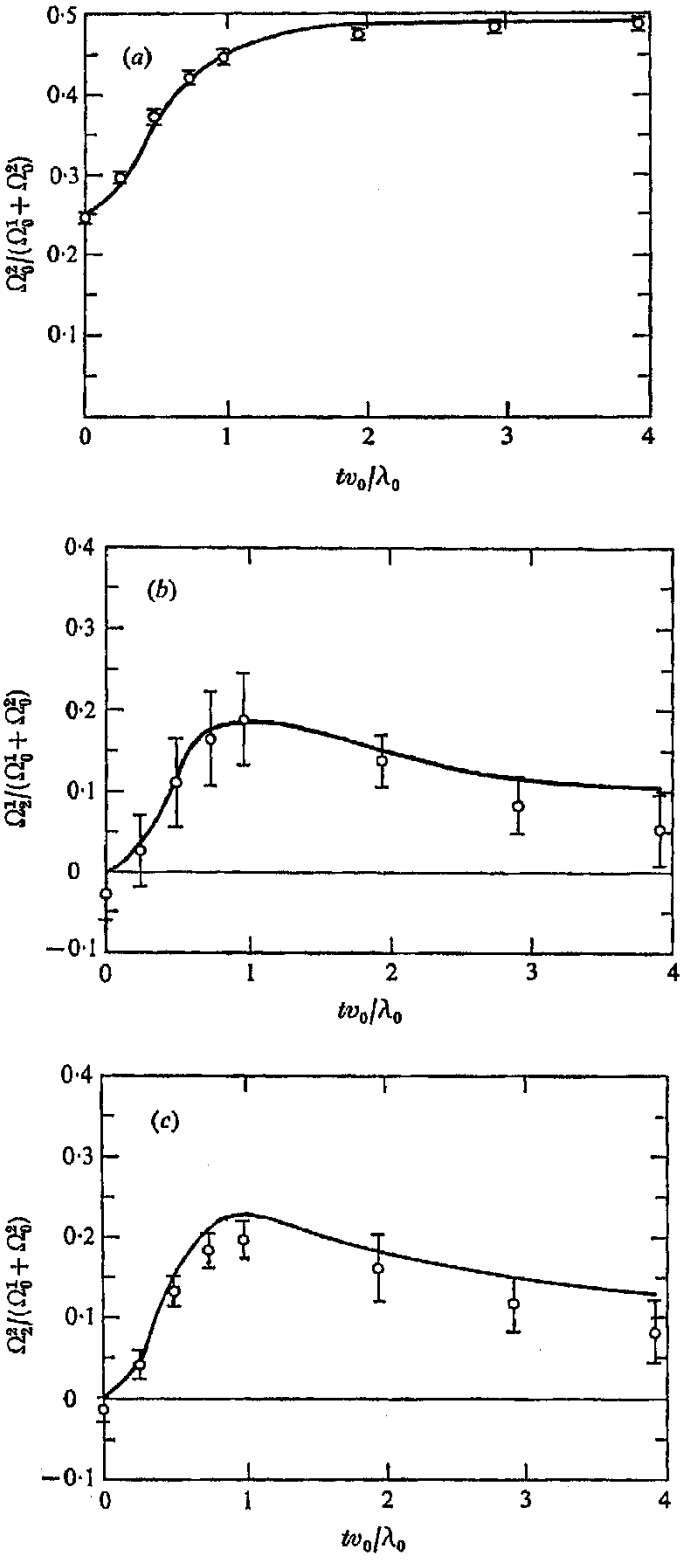

FIGURE 6. Dissipation moments *vs.* time for case *MA*.
(*a*) $\Omega_0^2/(\Omega_0^1+\Omega_0^2)$. (*b*) $\Omega_2^1/(\Omega_0^1+\Omega_0^2)$. (*c*) $\Omega_2^2/(\Omega_0^1+\Omega_0^2)$.

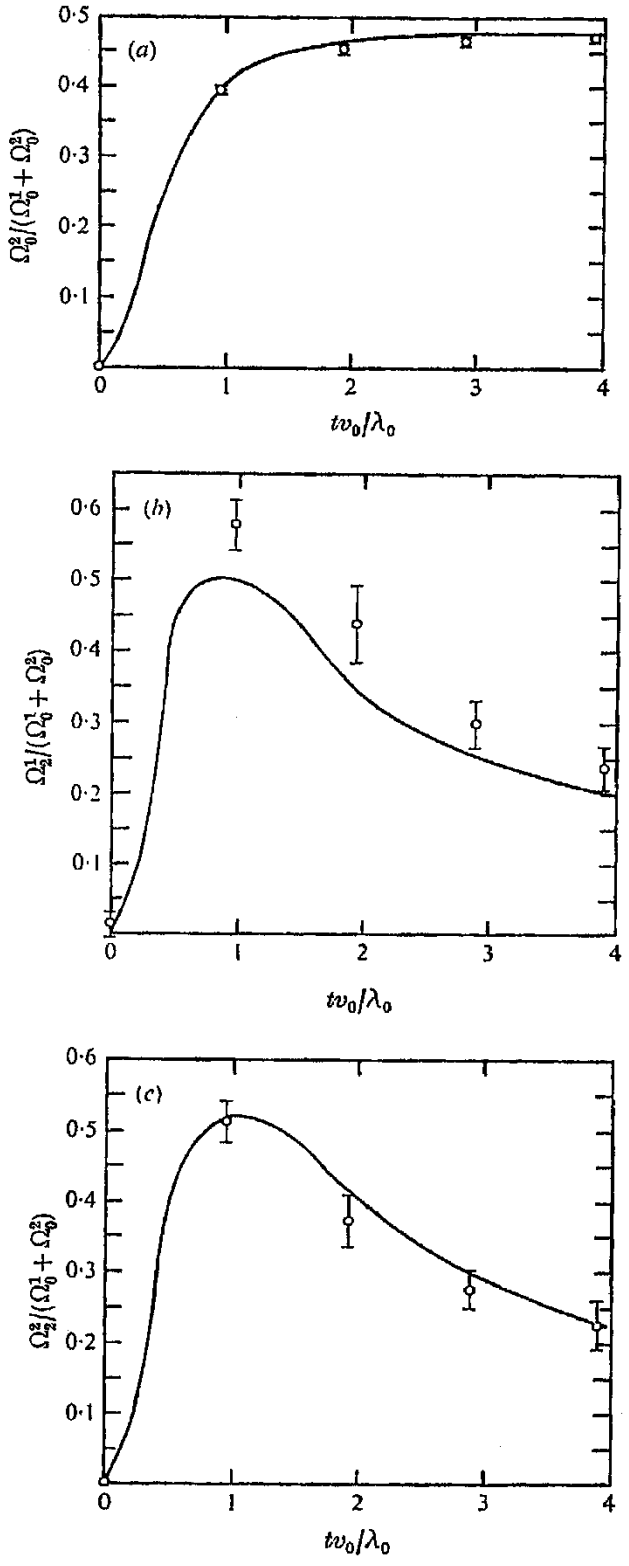

FIGURE 7. Dissipation moments *vs.* time for case *SA*.
(*a*) $\Omega_0^2/(\Omega_0^1+\Omega_0^2)$. (*b*) $\Omega_2^1/(\Omega_0^1+\Omega_0^2)$. (*c*) $\Omega_2^2/(\Omega_0^1+\Omega_0^2)$.

perhaps be explained by the presence of the upper wavenumber truncation, which reduces the nonlinear interaction in its neighbourhood.

We next compare results for energy and dissipation angular moments as defined by (2.21). The time evolution of the first two moments of energy (Φ_l^λ) and dissipation (Ω_l^λ) ($\lambda = 1, 2; l = 0, 2$) are shown in figures 5–7. All plotted values are normalized by $\Phi_0^1 + \Phi_0^2$ or $\Omega_0^1 + \Omega_0^2$ so that Φ_0^1 and Ω_0^1 need not be plotted, as they are complementary to Φ_0^2 and Ω_0^2, respectively. For isotropic turbulence the normalized moments are 0·5 for $l = 0$ and zero otherwise. The moments for $l = 0$ show the return to isotropy and we find very good agreement between the DSS and DIA. The second moments have been designed to be zero initially. We find, however, a strong departure to positive values during the transition from the anisotropic to the isotropic state. This is as found by Herring (1974) in some preliminary calculations. The physical meaning of this finding will be discussed later.

With respect to the higher moments, the DSS results not only show statistical uncertainties, but also a systematic deviation, in that they are negative initially and after long times. The latter effect is attributable to the rectangular rather than spherical grid used in wavenumber space, together with the general decrease in the modal energy as a function of k. This is easiest to see for a very coarse grid in two dimensions with $\mathbf{n} = (0, 1)$. Let us assume that we keep only the modes at $(0, 0)$, $(0, \pm 1)$, $(\pm 1, 0)$ and $(\pm 1, \pm 1)$ in wavenumber space. As the modal energy decreases as a function of k, it is smaller at $(\pm 1, \pm 1)$ than at $(\pm 1, 0)$. The energy value at $(0, 1)$ does not matter because of the weight $1-\mu^2$ appearing in (2.20). The least-squares fit for such a configuration is the same as if the energy were higher at $(\pm 1, 0)$ than at $(0, \pm 1)$ and we therefore get a negative second moment. This effect would not appear if the modal energy were uniform. Its appearance is also very much decreased if we use a finer resolution; therefore this error is smaller for the dissipation than for the energy moments, as can be seen by comparison of figures 5 and 6. In the latter figure the statistical uncertainties are smaller too, so that the DSS results are more significant with respect to the dissipation moments.

For case *MA* the DIA appears to overestimate slightly the build-up of the Φ_2 moments, although there is some uncertainty because of the rectangular-grid problem for the DSS noted above. For case *SA*, the DIA also slightly overestimates the Φ_2 moments (these are not shown) and underestimates the Ω_2^1 moment (figure 7*b*), while overestimating the Ω_2^2 moment. It is difficult to make much of these deviations, because of the statistical scatter. However, the overestimation of the Φ moments is consistent with a 'damming up' of energy in the $L = 2$ components caused by our neglect of modes with $L > 2$. The underestimation of the Ω_λ^2 moments for the *SA* run may be related to the fact that the DIA transfers too little energy to large-k regions (Herring & Kraichnan 1972). We note in this connexion that figure 8 finally shows that, indeed, the fourth moments are not negligible for case *SA* whereas they are sufficiently small for anisotropies that are weaker than in case *MA*.

We must point out, however, that the angular resolution is also effectively limited for the DSS, especially at low wavenumbers. This is so because of the

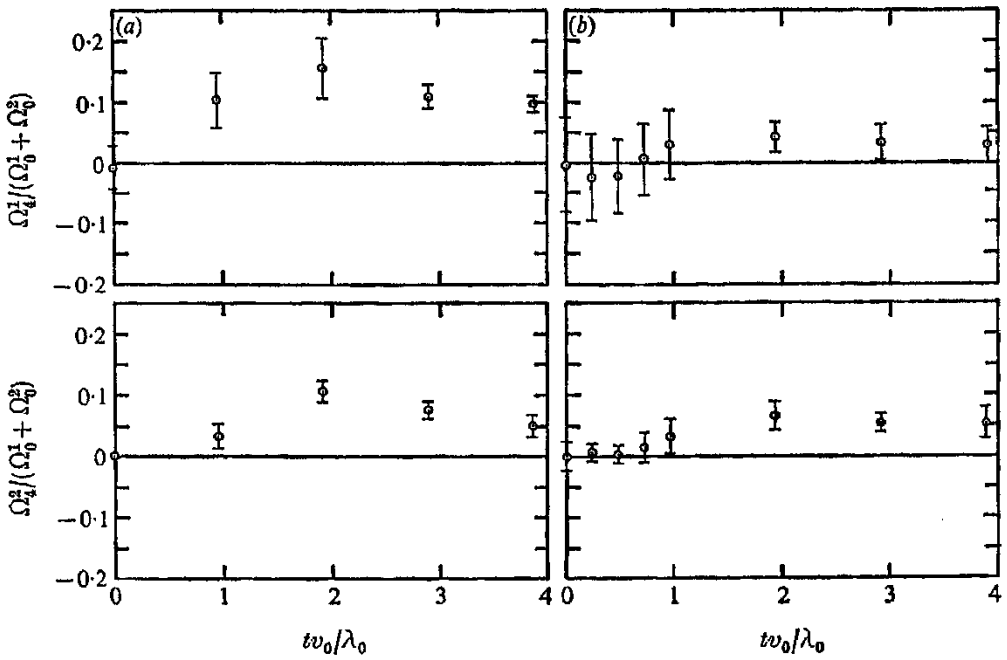

FIGURE 8. DSS results for the fourth angular dissipation moments $\Omega_4^\lambda/(\Omega_0^1+\Omega_0^2)$ for $\lambda = 1$, 2 and (*a*) case *SA* and (*b*) case *MA*.

small number of discrete wavenumber points that fall into a spherical shell. For this reason, the DSS estimate of the sixth-order energy moments (not shown) are not significant.

5. Physical interpretation of the second angular moments

The angular anisotropy that appears during the transition to the isotropic state has been found to be important as it reduces the return-to-isotropy rate (and probably also the dissipation rate) and increases the angular resolution requirements. It seems, therefore, worthwhile to give a physical picture of the evolution and meaning of, at least, the second angular moment.

For this purpose, let us first translate the $\hat{\Phi}^\lambda(\mathbf{k}, t, t)$ into energies

$$\langle \hat{u}_i(\mathbf{k}, t)\, \hat{u}_j(-\mathbf{k}, t)\rangle$$

as we are more used to thinking in these terms. From (2.2) we find for the energy, say E_{pp}, of the velocity components perpendicular to the axis of symmetry $\mathbf{n} = (0, 0, 1)$

$$\begin{aligned} E_{pp}(\mathbf{k}, t) &\equiv \langle \hat{u}_1(\mathbf{k}, t)\, \hat{u}_1(-\mathbf{k}, t)\rangle + \langle \hat{u}_2(\mathbf{k}, t)\, \hat{u}_2(-\mathbf{k}, t)\rangle \\ &= \hat{\Phi}^1(\mathbf{k}, t, t) + \hat{\Phi}^2(\mathbf{k}, t, t)\cos^2\theta \end{aligned} \tag{5.1}$$

and for the energy, say E_{nn}, of the velocity components parallel to the axis $\mathbf{n}$

$$E_{nn} = \hat{\Phi}^2(\mathbf{k}, t, t)\sin^2\theta. \tag{5.2}$$

Therefore, a schematic polar plot of the angular energy distribution for fixed $\mathbf{k}$ at $t = 0$ for $a = \frac{1}{3}$ looks like the full line in figure 9. The decrease of E_{nn} near

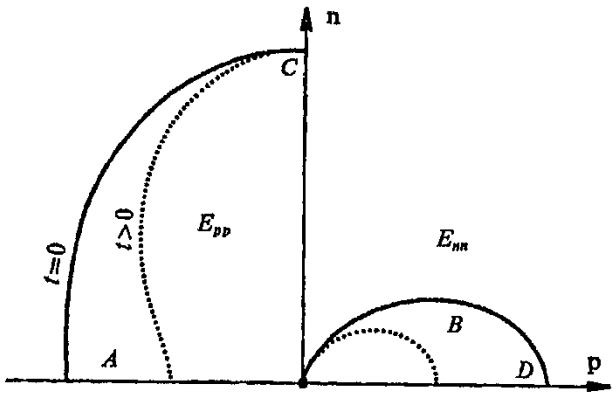

FIGURE 9. Schematic polar plot of the angular energy distribution with respect to the direction **n** of the axis of symmetry and any perpendicular direction **p** for the isotropic initial state (full curve) and at a later time (dotted curve) when positive second Φ_2^λ moments have evolved.

n and of E_{pp} near **p** is a consequence of the continuity equation $\mathbf{k}.\hat{\mathbf{u}} = 0$. The fact that the second moments Φ_2^λ for both $\lambda = 1$ and $\lambda = 2$ are positive after a short time means that the energy distribution becomes elongated in the direction of the axis **n**. This means that there is energy transfer out of region A into region B that is not only large near the **p** axis (region D) but also relatively large near the **n** axis. This energy transfer from region A to region B dominates until the energy in region A becomes equal to that in region D. Therefore, the second moments are larger for larger anisotropies. So far we have given a picture that is consistent with the numerical results.

We now offer a heuristic explanation of why the second moments evolve positively. We use Rotta's classical picture (see Rotta 1951, figure 2) of two moving fluid parcels which collide, both having the same speed but travelling in opposite directions, say the $\pm\mathbf{p}$ directions. This means that there is a large variation in the velocity component in the **p** direction and thus the Fourier decomposition shows a large amplitude at a wavenumber vector which has about the same direction as **p** (as, for example, in region A of figure 9). Such a collision causes the fluid between the two parcels to be squashed out into the normal, **n** direction, so that the magnitude and thus the energy of the **n** component is increased on the account of the **p** component. This increase has different signs on the two sides of the collision, i.e. the energy is fed into the **p** component at wavenumbers that are near to the **p** axis, like those in region B of figure 9.

This picture indicates that the energy transfer between different components is non-local in wavenumber vector space. From the same picture we expect negative second moments for $a > 0{\cdot}5$ and that is as found in Herring (1974, figure 1). We cannot, however, expect a complete symmetry between cases with anisotropies a and $1-a$ respectively, since the extreme case $a = 0$ corresponds to two-dimensional turbulence, while $a = 1$ means that energy is contained in the u_3 components only. Such a lack of symmetry can be seen from Herring's (1974) figures 1 and 2.

6. Technical aspects of the DIA

In this section, we discuss certain technical aspects of the DIA which are important in applications to anisotropic problems but not explicitly encountered in isotropic turbulence. We shall not attempt to describe the physical basis of the theory; readers interested in such questions should refer to the references cited in § 1.

6.1. *The coefficients $A_{\lambda\mu\nu}$ and $B_{\lambda\mu\nu}$*

Let us consider first the coefficients $A_{\lambda\mu\nu}(\mathbf{k}, \mathbf{p}, \mathbf{q})$ and $B_{\lambda\mu\nu}(\mathbf{k}, \mathbf{p}, \mathbf{q})$ entering (3.1) and (3.2). These quantities are too complex to examine here in any detail; instead, we present their $d\mathbf{p}$ integrals for certain selections of (λ, μ, ν) which are chosen so as to represent the initial second time derivative $\ddot{\Phi}(\mathbf{k}, 0)$ for isotropic angular distributions of $\hat{\Phi}^{\lambda}(\mathbf{k}, 0, 0)$. (According to (3.1), the first derivative is zero initially.) Certain of the analytic properties of these coefficients, together with a method for their accurate numerical evaluation, are presented in the appendix. The solid line in figure 10, for example, represents $\int A_{211}(\mathbf{k}, \mathbf{p}, \mathbf{q})\, \mathbf{d}\Omega_p$ as a function of $\mu = \cos\theta$ for $|\mathbf{k}| = |\mathbf{p}| = |\mathbf{q}|$. Here, $d\Omega_p$ is the angular part of the $d\mathbf{p}$ integration in (3.1), and represents a rotation of the (k, p, q) triangle about $\mathbf{k}$. The quantity depicted here is proportional to $\hat{\Phi}^2(\mathbf{k}, t, t)$ for the initial conditions $\Phi^2(\mathbf{k}, 0, 0) = 0$ and $\Phi^1(\mathbf{k}, 0, 0)$ and Φ^2 are spherically symmetric. The figure indicates strong transfer into the polar regions ($|\mu| \approx 1$), with smaller transfer into the equatorial region ($|\mu| \approx 0$). Such behaviour is consistent with the development of positive angular moments, found in both the DIA and the DSS calculations and explained in § 5. Also shown in figure 10 are equivalent results for $\int A_{122}(\mathbf{k}, \mathbf{p}, \mathbf{q}) d\Omega_p$ (dashed line). In this case, the transfer is more nearly into midlatitudes ($|\mu| \approx \frac{1}{2}$) than for the previous case. A curious feature here is the cusp which occurs at $\theta = \beta$ or γ, where β and γ are the interior angles opposite sides $\mathbf{p}$ and $\mathbf{q}$ of the triangle formed by (k, p, q). The figure indicates non-analytic behaviour of the angular distributions, and suggests that higher angular harmonics will be more pronounced in turbulence with prolate (positive second moment) rather than oblate angular distributions. This non-analytic behaviour is verified by the analytic study of the angular A and B integrals occurring in (3.1) and (3.2) given in the appendix. Thus it turns out that the integration which rotates the (k, p, q) triangle about $\mathbf{k}$ may be shown to yield, in general, functions of the polar angle θ with cusps at $\theta = (\beta, \gamma)$. More precisely, the resulting angular distribution is a rational function of four variables: $Z_1(\theta), \ldots, Z_4(\theta)$, where

$$\left.\begin{aligned} Z_1(\theta) &= \begin{cases} \cot\tfrac{1}{2}\beta \tan\tfrac{1}{2}\theta & \text{if} \quad \theta \leqq \beta, \\ -\tan\tfrac{1}{2}\beta \cot\tfrac{1}{2}\theta & \text{if} \quad \theta \geqq \beta, \end{cases} \\ Z_2(\theta) &= Z_1(\pi - \theta) \end{aligned}\right\} \tag{6.1}$$

and Z_3 and Z_4 are the same as Z_1 and Z_2 except that β is replaced by $-\gamma$. We thus must expect very rapid angular changes in the transfer for β or γ tending to zero or π.

The import of these remarks is that anisotropic turbulence in the DIA frame

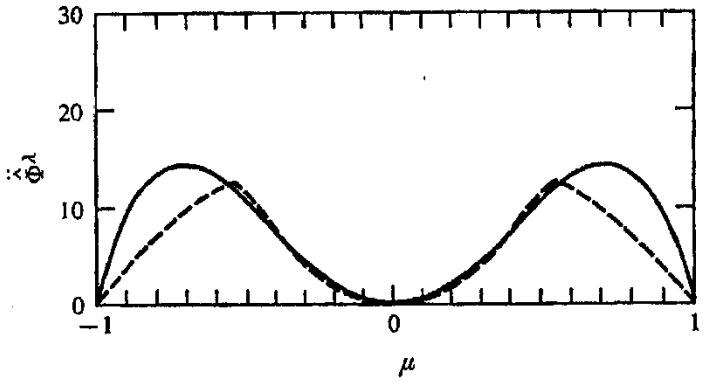

FIGURE 10. Angular distribution of input term in the DIA [equation (3.1)] as a function of the polar angle μ [see (2.7)]. Curves show the initial second time derivatives for $\hat{\Phi}^2$ (solid line) and $\hat{\Phi}^1$ (dashed line) for initial conditions $\hat{\Phi}^2 = 0$, $\hat{\Phi}^1$ independent of μ and $\hat{\Phi}^1 = 0$, $\hat{\Phi}^2$ independent of μ respectively. $k = p = q$ and the ordinate scale is arbitrary.

is more difficult to treat, numerically, than the otherwise equivalent isotropic turbulence problem, even after allowing for the increase in program size necessary to represent anisotropic aspects of the turbulence. Accurate representation of energy flow into the polar regions requires unexpectedly high angular harmonics.

6.2. *Green's function*

Turbulent relaxation, whereby the flow field 'forgets' its initial statistical state, is embodied in the DIA through the two-time functions $\hat{\Phi}^\lambda(\mathbf{k}, t, t')$ and $g^\lambda(\mathbf{k}, t, t')$. The latter describes the averaged response in the velocity field's Fourier components $\hat{\mathbf{u}}(\mathbf{k}, t)$ due to an infinitesimal perturbation at time t', and its time integral (from t' to t) may be thought of as the relaxation time of mode $\mathbf{k}$. It is the finite (and relatively small) value of this relaxation time as $t - t' \to \infty$ that saves the DIA from the fate of the quasi-normal theory (Ogura 1963; Orszag 1976), for which such integrals diverge, at least for sufficiently large Reynolds numbers. The characteristic time of $\hat{\Phi}^\lambda(\mathbf{k}, t, t')$ is typically somewhat longer than that of $g^\lambda(\mathbf{k}, t, t')$, particularly at large k, where transfer of energy implies that these modes partially 'inherit' the characteristic times of the region from which they receive their energy.

It is not clear on physical grounds how anisotropy should affect the behaviour of the $g^\lambda(\mathbf{k}, t, t')$ functions. Preliminary results by Herring (1974) suggested that anisotropy had little effect on $g^\lambda(\mathbf{k}, t, t')$; for the DIA truncated at $L = 0$, it was found that $g^1(\mathbf{k}, t, t') \cong g^2(\mathbf{k}, t, t')$, regardless of the initial degree of anisotropy. Such results could be of use in simplifying the DIA-type theory, so as to make high Reynolds number calculations more tractable. For example, Leslie (1973) has employed the hypothesis that the anisotropic relaxation effects may be entirely neglected in simplifying the DIA so as to apply it to shear flows.

Some results related to this point are presented in figure 11, which shows the $l = 0$ and $l = 2$ harmonics of $g^\lambda(\mathbf{k}, t, 0)$ for run MA. The $l = 0$ components are

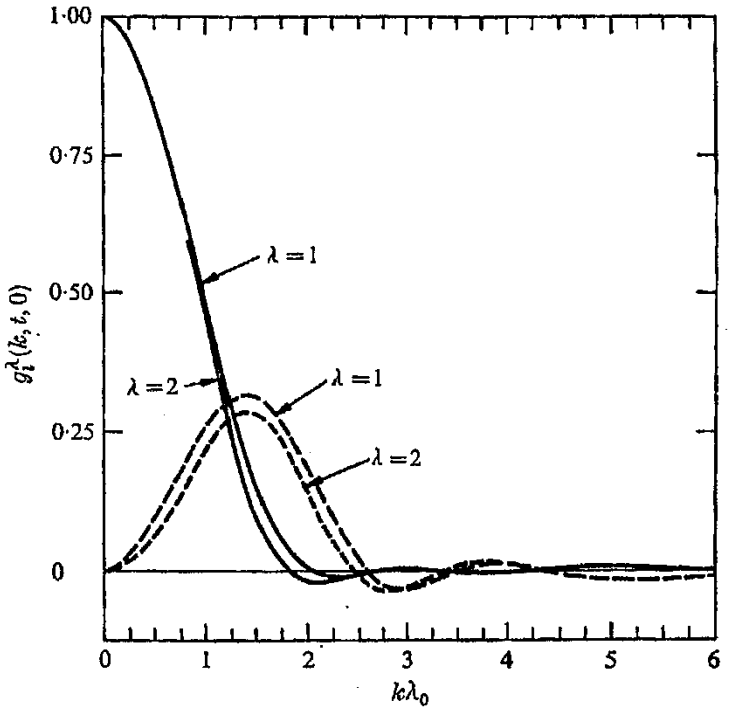

FIGURE 11. Green's functions $g_l^\lambda(k, t, 0)$. ——, $l = 0$; – – –, $l = 2$. Here, the index l designates the lth angular harmonic as defined by (2.18) of $g^\lambda(\mathbf{k}, t, 0)$, which satisfies (3.2). Curves are for $t = 3{\cdot}79\ \lambda_0/v_0$ and run MA.

given by the solid lines, the $l = 2$ components by the dashed lines. We note the close similarity between the $\lambda = 1$ and $\lambda = 2$ components, which extends the observation made in the preceding paragraph to the $L = 2$ approximation. On the other hand, the $l = 2$ component is not small compared with the $l = 0$ component, so that it is not clear that such terms may be neglected with impunity. To check this point, we have rerun case MA with $g_2^\lambda(\mathbf{k}, t, t') = 0$ for all (t, t'). The results of this run indicate a small but significant contribution of the $l = 2$ component of $g^\lambda(\mathbf{k}, t, t')$ to the evolution of anisotropy. In particular, the value of $C'(t)$ increased by about 15 %, and also the spectral measure of anisotropy $E_{33}(k, t)/E_{11}(k, t)$ increased by 2–4 %, with the larger increase at large k, where at later times it became slightly larger than unity.

7. Concluding discussion

We must keep in mind that the DIA is a model that describes turbulence only approximately and has deficiencies, some of which have been pointed out earlier (Kraichnan 1964). Nevertheless, it is a fully self-consistent (computable) analytical turbulence theory (Orszag 1976). The DSS method (and similar direct numerical simulation schemes), on the other hand, integrates the Navier–Stokes equations directly and should give accurate solutions if the resolution (L_{box} and k_{max}) is sufficiently high. With respect to turbulence statistics it has the

disadvantage that large ensembles of results must be produced from which the statistical information can be deduced. This is, in principle, a more time-consuming procedure than the DIA. On the other hand, the DSS allows one to compute any type of correlation, e.g. fifth-order statistical moments, which are beyond the scope of the present version of the DIA, which treats moments up to only the third order. Also, the numerical solution of the DIA equations is not at all trivial and the present computing time for one DIA run with $L = 2$ is of the same order as one realization produced by the DSS, although this statement is certainly preliminary. It would appear necessary to improve the present DIA numerical analysis before more complicated, and practical flow problems (e.g. large Reynolds number channel flow) are amenable to this type of analytical turbulence theory.

The present results indicate that the numerical analysis of the DIA should resolve also the fourth angular moment in order to compute Rotta's constant accurately. This is definitely necessary for strong anisotropies. It would also be necessary for all flows with directional forces like buoyancy in natural convection or the Lorentz force in a flow of a conducting fluid under an imposed magnetic field (Moreau 1968).

Such problems may in principle be studied without any difficulty by means of the DSS method, the only basic limitation being the available computer resources. The present study has shown that these limitations in fact exclude application of the DSS for small anisotropies.†

Both methods are limited with respect to the range of Reynolds numbers that can be studied with sufficient accuracy. Subgrid-scale models (Schumann 1975) or appropriately changed statistical theories (Kraichnan 1971) must be used for high Reynolds number flows.

This work was done while Ulrich Schumann was with the Advanced Study Program at the National Center for Atmospheric Research, which is sponsored by the National Science Foundation. It is in part an extension of previous work done in collaboration with Dr G. S. Patterson, whom we should like to thank for several discussions. We thank Sandra Fuller for programming the evaluation of the DIA coefficients given in the appendix.

Appendix

We sketch here some of the essential details in the evaluation of the angular integrations in (3.1) and (3.2). Our methods follow those of Herring (1974), but we show here how to replace the strictly numerical scheme presented there by a semi-analytic method with greatly improved overall accuracy. First, substitute the angular expansion (2.18) for $\hat{\Phi}^\lambda(\mathbf{k}, t, t')$ and an equivalent one for $g^\lambda(\mathbf{k}, t, t')$ into (3.1) and (3.2). There result equations of motion for $\hat{\Phi}^\lambda_l(k, t, t')$ and $g^\lambda_l(k, t, t')$ upon projecting (3.1) and (3.2) onto $P_l(\mu_k), \mu_k = \cos\theta_k = \mathbf{k}.\mathbf{n}/k$. (We recall that

† Professor D. C. Leslie (private communication) has pointed out that this difficulty may be obviated if one is able to store and compute the unaveraged isotropic infinitesimal response function in the DSS procedure.

the **k** dependence of $\hat{\Phi}^\lambda$ and g^λ is (k, μ_k) since the turbulence has axisymmetry.) These equations are (13) and (14) of Herring (1974), and we record them here for completeness:

$$d\hat{\Phi}_l^\lambda(k,t,t')/dt + \nu k^2 \hat{\Phi}_l^\lambda(k,t,t') = \sum_{l',\mu,\nu} \int_\Delta dp\, dq\, A_{\lambda\mu\nu}^{ll'mn}(k,p,q) \int_0^{t'} ds\, g_{l'}^\lambda(k,t',s)\, \hat{\Phi}_m^\mu(p,t,s)\, \hat{\Phi}_n^\nu(q,t,s) + \sum_{l,\mu,\nu} \int_\Delta dp\, dq\, B_{\lambda\mu\nu}^{ll'mn}(k,p,q) \int_0^t ds\, \hat{\Phi}_l^\lambda(k,t',s)\, g_m^\mu(p,t,s)\, \hat{\Phi}_n^\nu(q,t,s), \quad (A\,1)$$

where

$$A_{\lambda\mu\nu}^{ll'mn}(k,p,q) = \left(\frac{2l+1}{2}\right)\frac{pq}{k} \times \int_0^{2\pi} d\phi_p \int_{-1}^{1} d\mu_k\, P_l(\mu_k)\, P(\mu_k) \times P_m(\mu_p)\, P_n(\mu_q)\, A_{\lambda\mu\nu}(\mathbf{k},\mathbf{p},\mathbf{k}-\mathbf{p}), \quad (A\,2)$$

$$B^{ll'mn}(k,p,q) = \left(\frac{2l+1}{2}\right)\frac{pq}{k} \times \int_0^{2\pi} d\phi_p \int_{-1}^{1} d\mu_k\, P_l(\mu_k)\, P_\nu(\mu_k) \times P_m(\mu_p)\, P_n(\mu_q)\, B_{\lambda\mu\nu}(\mathbf{k},\mathbf{p},\mathbf{k}-\mathbf{p}). \quad (A\,3)$$

The expressions for $A_{\lambda\mu\nu}$ and $B_{\lambda\mu\nu}$ are

$$\left.\begin{aligned} A_{\lambda\mu\nu}(\mathbf{k},\mathbf{p},\mathbf{q}) &= |F_{\lambda\mu\nu}(\mathbf{k},\mathbf{p},\mathbf{q})|^2, \\ B_{\lambda\mu\nu}(\mathbf{k},\mathbf{p},\mathbf{q}) &= F_{\lambda\mu\nu}(\mathbf{k},\mathbf{p},\mathbf{q})\, L_{\lambda\mu\nu}(\mathbf{k},\mathbf{p},\mathbf{q}), \end{aligned}\right\} \quad (A\,4)$$

where $$F_{\lambda\mu\nu}(\mathbf{k},\mathbf{p},\mathbf{q}) = -\tfrac{1}{2}i\{[\mathbf{e}^\lambda(\mathbf{k}).\mathbf{e}^\nu(\mathbf{q})][\mathbf{q}.\mathbf{e}^\mu(\mathbf{p})] + [\mathbf{e}^\lambda(\mathbf{k}).\mathbf{e}^\mu(\mathbf{p})][\mathbf{p}.\mathbf{e}^\nu(\mathbf{q})]\} \quad (A\,5)$$

and $$L_{\lambda\mu\nu}(\mathbf{k},\mathbf{p},\mathbf{q}) = \tfrac{1}{2}i\{[\mathbf{e}^\mu(\mathbf{p}).\mathbf{e}^\nu(\mathbf{q})][\mathbf{q}.\mathbf{e}^\lambda(\mathbf{k})] - [\mathbf{e}^\mu(\mathbf{p}).\mathbf{e}^\lambda(\mathbf{k})][\mathbf{k}.\mathbf{e}^\nu(\mathbf{q})]\}. \quad (A\,6)$$

Here, the unit vectors $\mathbf{e}^\lambda(\mathbf{k})$ are given by (2.3). In (A 2), $\int d\phi_p$ is the angular integration that spins the triangle formed by $(k,\ p,\ q = |\mathbf{k}-\mathbf{p}|)$ about **k**. Equation (A 2) results from writing the $d\mathbf{p}$ integration in the convolution integral entering the DIA as $(pq/k)\, dp\, dp$, and choosing the polar **p** axis as **k**. Note that we have fixed the azimuthal k angle ϕ_k at zero, thereby restricting the present analysis to axisymmetrical turbulence. We now given an analytical method for the $d\phi_p$ integration, and state the numerical method for effecting the $d\mu_k$ integration.

To this end, we first note that the direction cosines entering (A 2) may be written as

$$\mu_k = \cos\theta, \quad (A\,7)$$

$$\mu_p = \cos\gamma\cos\theta - \cos\phi\sin\gamma\sin\theta \equiv \cos p, \quad (A\,8)$$

$$\mu_q \equiv (\mathbf{k}-\mathbf{p}).\mathbf{n}/|\mathbf{k}-\mathbf{p}| = \cos\theta\cos\beta + \cos\phi\sin\beta\sin\theta \equiv \cos q. \quad (A\,9)$$

In (A 8) and (A 9) (and in subsequent equations) we have dropped the subscript p on ϕ, for notational convenience. Here β and γ are interior angles opposite **p** and **q** and α is the exterior angle opposite **k** in the triangle formed by (k, p, q). Consider now the $d\phi$ integral in (A 2), which we denote generically as I_ϕ. Recognizing the form of (A 2), and the unitarity of the $\mathbf{e}^\lambda(\mathbf{k})$, this may be written as

$$\sin^2\theta\, I_\phi = \int_0^{2\pi} d\phi (1-\mu_p^2)^{-1} (1-\mu_q^2)^{-1} H(\sin\phi, \cos\phi), \quad (A\,10)$$

$$
\begin{aligned}
\mathbf{f}^1(\mathbf{k}).\mathbf{f}^1(\mathbf{q}) &= \cos\beta - \cos\theta\cos q\\
\mathbf{f}^1(\mathbf{k}).\mathbf{f}^2(\mathbf{q}) &= -\sin\theta\sin\phi\sin\beta\cos q\\
\mathbf{f}^2(\mathbf{k}).\mathbf{f}^1(\mathbf{q}) &= \sin\theta\sin\phi\cos\theta\sin\beta\\
\mathbf{f}^2(\mathbf{k}).\mathbf{f}^2(\mathbf{q}) &= \cos\beta(\cos\beta - \cos\theta\cos q) + \sin^2\theta\sin^2\phi\sin^2\beta\\
\mathbf{f}^1(\mathbf{k}).\mathbf{q} &= -q\sin\theta\sin\phi\sin\beta\\
\mathbf{f}^2(\mathbf{k}).\mathbf{q} &= q(\cos\beta\cos\theta - \cos q)\\
\mathbf{f}^1(\mathbf{q}).\mathbf{k} &= k\sin\theta\sin\phi\sin\beta\\
\mathbf{f}^2(\mathbf{q}).\mathbf{k} &= k(\cos\beta\cos q - \cos\theta)\\
\mathbf{f}^1(\mathbf{k}).\mathbf{f}^1(\mathbf{p}) &= \cos\gamma - \cos\theta\cos p\\
\mathbf{f}^1(\mathbf{k}).\mathbf{f}^2(\mathbf{p}) &= \cos p\sin\theta\sin\phi\sin\gamma\\
\mathbf{f}^1(\mathbf{k}).\mathbf{f}^2(\mathbf{p}) &= -\cos\theta\sin\theta\sin\phi\sin\gamma\\
\mathbf{f}^2(\mathbf{k}).\mathbf{f}^2(\mathbf{p}) &= \cos\gamma(\cos\gamma - \cos\theta\cos p) + \sin^2\theta\sin^2\phi\sin^2\gamma\\
\mathbf{f}^1(\mathbf{k}).\mathbf{p} &= p\sin\theta\sin\phi\sin\gamma\\
\mathbf{f}^2(\mathbf{k}).\mathbf{p} &= p(\cos\theta\cos\gamma - \cos p)\\
\mathbf{f}^1(\mathbf{p}).\mathbf{k} &= -k\sin\theta\sin\phi\sin\gamma\\
\mathbf{f}^2(\mathbf{p}).\mathbf{k} &= k(\cos p\cos\gamma - \cos\theta)\\
\mathbf{f}^1(\mathbf{p}).\mathbf{f}^1(\mathbf{q}) &= \cos\alpha - \cos p\cos q\\
\mathbf{f}^1(\mathbf{p}).\mathbf{f}^2(\mathbf{q}) &= -\cos q\sin\theta\sin\phi\sin\alpha\\
\mathbf{f}^2(\mathbf{p}).\mathbf{f}^1(\mathbf{q}) &= \cos p\sin\theta\sin\phi\sin\alpha\\
\mathbf{f}^2(\mathbf{p}).\mathbf{f}^2(\mathbf{q}) &= \cos\alpha(\cos\alpha - \cos p\cos q) + \sin^2\theta\sin^2\phi\sin^2\alpha\\
\mathbf{f}^1(\mathbf{q}).\mathbf{p} &= k\sin\theta\sin\phi\sin\beta\\
\mathbf{f}^2(\mathbf{q}).\mathbf{p} &= p(\cos\alpha\cos q - \cos p)\\
\mathbf{f}^1(\mathbf{p}).\mathbf{q} &= -k\sin\theta\sin\phi\sin\gamma\\
\mathbf{f}^2(\mathbf{p}).\mathbf{q} &= q(\cos\alpha\cos p - \cos q)
\end{aligned}
$$

TABLE 2

where $H(x, y)$ is polynomial in its arguments. Since, according to (A 8) and (A 9), μ_p and μ_q are linear in $\cos\phi$, it follows that the transformation $Z = \exp(i\phi)$ permits (A 10) to be evaluated by residues. The result is

$$I_\phi = [4/(\sin^3\theta\sin\beta\sin\gamma)]^2 \sum_{n=0}^{N} J_n(\theta)\,\Omega_n(\theta), \tag{A 11}$$

where

$$J_n(\theta) = 2\pi \sum_{l=1}^{4} Z_l^{n+3} \prod_{l+j}^{8} (Z_l - Z_j)^{-1} \tag{A 12}$$

and

$$\Omega_n(\theta) = \operatorname*{coeff}_{(Z^n)} [H(-\tfrac{1}{2}i(Z - Z^{-1}),\quad \tfrac{1}{2}(Z + Z^{-1})], \tag{A 13}$$

$$
\left.
\begin{aligned}
Z_1 &= (\tan\tfrac{1}{2}\beta\cot\tfrac{1}{2}\theta \text{ or reciprocal}),\\
Z_2 &= (-\cot\tfrac{1}{2}\beta\tan\tfrac{1}{2}\theta \text{ or reciprocal}),\\
Z_3 &= (-\tan\tfrac{1}{2}\gamma\cot\tfrac{1}{2}\theta \text{ or reciprocal}),\\
Z_4 &= (\cot\tfrac{1}{2}\gamma\tan\tfrac{1}{2}\theta \text{ or reciprocal}),\\
Z_{n+4} &= 1/Z_n \quad (n = 1, 2, 3, 4).
\end{aligned}
\right\} \tag{A 14}
$$

In (A 11), N is the maximum power of Z in $H(-\frac{1}{2}i(Z - Z^{-1}), \frac{1}{2}(Z + Z^{-1}))$. In the definitions (A 14) for the Z_n, we take that right-hand side whose absolute value is less than unity. It remains to work out the polynomials H. (Note that there are as many H's as specifications $(l, l', m, n, \lambda, \mu, \nu)$.) According to (A 4)–(A 6), (A 8) and (A 9), the $H(\sin\phi, \cos\phi)$'s are simply related to (A 4) if unnormalized vectors $\mathbf{f}^\lambda(\mathbf{k})$ defined by

$$\mathbf{f}^\lambda(\mathbf{k}) = \sin\theta\,\mathbf{e}^\lambda(\mathbf{k}) \tag{A 15}$$

replace the $\mathbf{e}^\lambda(\mathbf{k})$ entering (A 4)–(A 6). The relevant dot products entering (A 5) and (A 6) are listed in table 2. To get the H's we use table 2 to evaluate dot products in (A 5) and (A 6), and then substitute (A 4) into (A 2) and (A 3), using (A 8) and (A 9) for μ_p and μ_q. The algebraic reduction to obtain equation (A 13) for $\Omega_n(\theta)$ seems formidable, but is avoidable if we use the observation that $\Omega_n(\theta)$ may be equivalently written as

$$\Omega_n(\theta) = \int_{-1}^{1} T_n(x)\,(1-x^2)^{-\frac{1}{2}}\,dx\,[H((1-x^2)^{\frac{1}{2}}, x) + H(-(1-x^2)^{\frac{1}{2}}, x)], \quad \text{(A 16)}$$

where $T_n = \cos(n \arccos x)$, for which the Gauss–Tschebyschev integration method (of order N) is exact, since H is a polynomial of degree $\leqslant N$. Equation (A 16) then permits the algebra to be done by computer.

At this stage, we have an exact expression for the right-hand sides of (A 2) and (A 3), prior to the $d\mu_k$ integration. In performing this last integration, some care must be exercised, since according to (A 11)–(A 14), the angular distributions may in general have cusps at $\theta = \beta$ or $\theta = \gamma$. Our numerical procedure here is to divide the μ_k interval $(-1, 1)$ into subregions $(-1, -\max(|\cos\beta|, |\cos\gamma|))$, $(-\max(|\cos\beta|, |\cos\gamma|), \min(|\cos\beta|, |\cos\gamma|))$ and $(\min(|\cos\beta|, |\cos\gamma|), +1)$, and perform the $d\mu_k$ integrations on these subregions by Gauss–Legendre quadrature.

Finally, we note that the restriction of axisymmetry may be removed simply by reintroducing the azimuthal $\mathbf{k}$ angle ϕ_k into both the angular expansion functions (i.e. replace $P_l(\cos\theta_k)$ by $Y_l^m(\cos\theta_k, \phi_k)$) and the angular expansions of the scalar $\hat{\Phi}^\lambda(\mathbf{k})$ functions.

REFERENCES

Herring, J. R. 1974 Approach of axisymmetric turbulence to isotropy. *Phys. Fluids*, **17**, 859–872. Erratum, *Phys. Fluids*, **19**, 167.

Herring, J. R. & Kraichnan, R. H. 1972 Comparison of some approximations for isotropic turbulence. In *Lecture notes in Physics, vol. 12, Statistical Models and Turbulence*, pp. 148–194. Springer.

Herring, J. R., Orzag, S. A., Kraichnan, R. H. & Fox, D. G. 1974 Decay of two-dimensional homogeneous turbulence. *J. Fluid Mech.* **66**, 417–444.

Kraichnan, R. H. 1959 The structure of isotropic turbulence at very high Reynolds numbers. *J. Fluid Mech.* **5**, 497–543.

Kraichnan, R. H. 1964 Decay of isotropic turbulence in the direct-interaction approximation. *Phys. Fluids*, **7**, 1030–1048.

Kraichnan, R. H. 1971 An almost-Markovian Galilean-invariant turbulence model. *J. Fluid Mech.* **47**, 513–524.

Launder, B. E., Morse, A., Rodi, W. & Spalding, D. B. 1973 Prediction of free shear flows – a comparison of the performance of six turbulence models. In *Proc. Langley Working Conf. Free Turbulent Shear Flows, N.A.S.A. Special Paper*, SP-321, pp. 361–422.

Leslie, D. C. 1973 *Developments in the Theory of Turbulence*. Oxford: Clarendon Press.

Moreau, R. 1968 On magnetohydrodynamic turbulence. *Proc. Symp. Turbulence of Fluids & Plasmas, Polytech. Inst. Brooklyn*, pp. 359–372.

Ogura, Y. 1963 A consequence of the zero-fourth-cumulant approximation in the decay of isotropic turbulence. *J. Fluid Mech.* **16**, 33–40.

Orszag, S. A. 1976 *Lectures on the Statistical Theory of Turbulence, Proc. Les Houches Summer School.* Springer.

Orszag, S. A. & Patterson, G. S. 1972 Numerical simulation of turbulence. In *Lecture notes in Physics, vol.* 12, *Statistical Models and Turbulence*, pp. 127–147. Springer.

Riley, J. J. & Patterson, G. S. 1974 Diffusion experiments with numerically integrated isotropic turbulence. *Phys. Fluids.* **17**, 292–297.

Rotta, J. 1951 Statistische Theorie nichthomogener Turbulenz. *Z. Phys.* **129**, 547–572.

Schumann, U. 1975 Subgrid scale model for finite difference simulations of turbulent flows in plane channels and annuli. *J. Comp. Phys.* **18**, 376–404.

Schumann, U. & Patterson, G. S. 1976*a* Numerical study of pressure and velocity fluctuations in nearly isotropic turbulence. Submitted to *J. Fluid Mech.*

Schumann, U. & Patterson, G. S. 1976*b* Numerical study of the return of axisymmetric turbulence to isotropy. Submitted to *J. Fluid Mech.*